Brillouin scattering in diamond*

M. H. Grimsditch and A. K. Ramdas

Department of Physics, Purdue University, West Lafayette, Indiana 47907

(Received 16 December 1974)

The Brillouin spectrum of diamond excited with either the Ar^+ or He-Ne laser radiation is measured with a triple-passed piezoelectrically scanned Fabry-Perot interferometer. The polarization features and the selection rules have been verified for a number of scattering geometries. From the measured frequency shifts of the Brillouin components, the following values are obtained for the elastic moduli: $c_{11} = 10.764 \pm 0.002$, $c_{12} = 1.252 \pm 0.023$, and $c_{44} = 5.774 \pm 0.014$ in units of 10^{12} dyn/cm^2. The relative intensities of the observed Brillouin components for a variety of scattering geometries are consistent with the following elasto-optic contants: $p_{44} = -0.172$ and p_{11}-$p_{12} = -0.292$ determined by Denning *et al.* and $p_{11} + 2p_{12} = -0.1640$ obtained by Schneider. From a comparison of the Brillouin spectrum and the Raman spectrum associated with the zone-center optical phonon, observed under identical conditions, we obtain a value for the single independent component characterizing the Raman tensor per unit cell, viz., $|a| = 4.4 \pm 0.3$ Å^2.

I. INTRODUCTION

Spectral analysis of light scattered by crystals, Raman and Brillouin scattering, is now a well-established technique for investigating phonons in crystals. As is well known, the Raman effect associated with the one-phonon process involves zone-center optical phonons, whereas that arising from multiphonon processes yields information on the critical points in the phonon dispersion curves throughout the Brillouin zone.[1] On the other hand, Brillouin scattering arises from the interaction of light with phonons of the acoustic branch close to the zone center.[2] Diamond, an elemental crystal of considerable importance in solid-state physics in view of the simplicity of its structure and as a prototype of covalent crystals, is transparent throughout the visible and near-ultraviolet region of the spectrum. It is thus eminently suited for light-scattering studies. The first- and second-order Raman spectra of diamond have been the subject of several investigations, the most recent one being that of Solin and Ramdas,[3] who used laser excitation and photoelectric detection. They were able to interpret their results in terms of the critical points of the phonon dispersion curves as determined by inelastic neutron scattering.[4] The strong covalent bonding results in a large frequency for the zone-center Raman-active, infrared-inactive, triply degenerate optical phonon.[3] For the same reason, the elastic constants of diamond are some of the largest known for any material and thus lead to Brillouin components with large frequency shifts. Indeed, Brillouin-scattering experiments were carried out by Krishnan,[5] Chandrasekharan,[6] and Krishnan *et al.*[7] using the 2537-Å resonance radiation of mercury (Rasetti technique) and a high-dispersion quartz spectrograph. The elastic constants determined from their measurements differ somewhat from the most recent determinations of McSkimin and Andreatch,[8] who used the ultrasonic-pulse technique. In this context, it appears to us that a redetermination of the elastic constants from a Brillouin-scattering investigation using laser excitation and a high-resolution Fabry-Perot interferometer is worthwhile. Also, the values for the elasto-optic constants for diamond which appear in the literature[9] differ among themselves significantly. The phenomenological theory of Brillouin scattering gives intensities of Brillouin components in terms of elasto-optic constants.[2] Thus there is considerable interest in reliable intensity measurements of Brillouin components which are attainable with photoelectric detection. The purpose of the present paper is to report the results of an investigation[10] undertaken with the above considerations.

II. THEORY

The energies of the phonons involved in Brillouin scattering studied with visible radiation are usually much smaller than the thermal energy; also, the wavelength of these phonons is much longer than the interatomic distances. A continuum classical description of the phenomenon is therefore generally adequate. This approach is well described in the literature,[2,11,12] and in this section we summarize the results relevant for comparison with our experiments. From the classical point of view the scattering is a result of a Bragg reflection from the optical stratifications produced by the long-wavelength acoustic phonons in the medium; the Doppler shifts associated with these "moving mirrors" produce the Brillouin components. For given incident (i) and scattered (s) directions, the frequency shifts $\Delta\omega$ of the Brillouin components in a cubic crystal are given by

$$\Delta\omega = \pm 2\omega_L n(v_s/c)\sin(\tfrac{1}{2}\theta) \ . \tag{1}$$

Here ω_L is the excitation frequency, n the refractive index, c the velocity of light in vacuum, θ the scattering angle, and v_s the velocity of the appropriate sound wave responsible for the Bragg reflection. For a general direction of propagation, there will be three values for v_s corresponding to two quasitransverse (QT) and one quasilongitudinal (QL) sound waves; v_s in turn can be written as $\sqrt{X/\rho}$, where X is an appropriate combination of the elastic moduli (c_{ij}) and ρ is the density. The intensity of a Brillouin component is obtained from the changes in the refractive index produced by the strains generated by the sound wave. The changes in refractive index are related to the strains through the elasto-optic constants (p_{ij}). The analysis based on the above considerations leads to a scattering tensor T characterizing a given phonon[2]; these are listed in Table I for simple crystallographic directions. The intensities are derived from this tensor using the following equation:

$$I = \text{const} \frac{(\hat{e}_s \cdot T \cdot \hat{e}_i)^2}{X} \quad , \tag{2}$$

where $\hat{e}_s$ and $\hat{e}_i$ are unit vectors along the polarization direction of the scattered and incident light, respectively, and the constant of proportionality is a function of the refractive index, temperature, and the scattered frequency. In Table II we give the intensities of the Brillouin components for the right-angle scattering configuration with incident and scattered light along [110] and [$\bar{1}$10], respectively; this is a geometry we have examined experimentally in some detail.

III. EXPERIMENTAL PROCEDURE AND APPARATUS

Three oriented diamonds were used in this investigation; they are natural crystals, two of type IIb and one of type IIa in the form of rectangular parallelepipeds, all six faces being polished.[13] The two type-IIb specimens have (001), (110), ($1\bar{1}0$) and (111), ($1\bar{1}0$), ($11\bar{2}$) faces, respectively. The type-IIa specimen has $\{100\}$ faces. The faces are within 1° or 2° from the specified crystallographic directions.

The Brillouin spectra were excited with a coherent-radiation Ar$^+$ laser (Model 52A). The 5145- and 4880-Å lines were employed and were single moded when necessary with a model-490 oven-stabilized etalon in the laser cavity. The scattered radiation was analyzed with a piezoelectrically scanned Fabry-Perot interferometer.[14] This instrument was triple passed following the technique described by Sandercock.[15] Two sets of matched etalon plates were used; both pairs had a broad band reflection coating for the range between 4880 and 6300 Å. The pair of higher reflectivity [(94 ± 3)%] was used for the intensity measurements; these measurements were made with large free-spectral ranges (~ 10 cm^{-1}), where large pinholes could be used to offset the loss of intensity due to absorption. The other pair, of lower reflectivity [(86.5 ± 1.5)%], was used with small free-spectral ranges (~ 0.5 cm^{-1}); in these cases small pinholes had to be used and the consequent loss of intensity was made up for by the lower reflectivity of the mirrors. The latter measurements were made to obtain the frequency shifts of the Brillouin components with high precision. The relative intensities of the Brillouin lines to the Raman line were obtained using a 1-m double monochromator.[16] The detection system consisted of a cooled photomultiplier and associated photon-counting electronics.[17] An RCA 7265 and an ITT FW-130 photomultipliers were used in the Fabry-Perot and the double monochromator, respectively. In many experiments, an I_2 filter was utilized to suppress the unshifted parasitic radiation.[18] This filter was used only in experiments with poor specimens or with difficult scattering geometries; only frequency shifts were deduced from these experiments since the intensities were distorted by the filter. In all the experiments performed with the Fabry-Perot interferometer, a narrow-band interference filter with a bandwidth of ~ 10 Å was used to restrict the scattered radiation analyzed to the Brillouin components and to exclude the Raman spectrum.

The free-spectral range of the Fabry-Perot interferometer was determined by the following procedure. The wave-number difference $\Delta\tilde{\nu}$ of two spectral lines analyzed by the interferometer is given by

$$\Delta\tilde{\nu} = (\Delta n + p)R_{FS} \quad , \tag{3}$$

where Δn is the difference in interference order of these lines observed within the same free-spectral range, p the fractional order difference, and R_{FS} the free-spectral range. From a sufficiently accurate knowledge of the free-spectral range, Δn, an integer, can be determined unambiguously for a given $\Delta\tilde{\nu}$. Of course, to achieve this, the choice of $\Delta\tilde{\nu}$ has to be compatible with the accuracy with which R_{FS} is known. Now the experimental value of p and the Δn as deduced above yields, using Eq. (3), a value for R_{FS} which is more accurate than the initial estimate. This procedure can now be repeated successively with pairs of lines with larger and larger $\Delta\tilde{\nu}$. In our experiments, we obtained the first estimate of R_{FS} by measuring the plate separation with a precision calipers. Spectral lines of known wavelengths were selected for their sharpness and for their convenient frequency differences.[19] By following this iterative procedure, R_{FS} could be determined with an accuracy ranging from 0.05 to 0.01%.

TABLE I. Scattering tensor (T), $X = v_s^2 \rho$, and the polarization vector $(\vec{u})$ of phonons traveling along $\vec{q}$.

$\vec{q}$	X	T	$\vec{u}$
[100]	c_{11}	$2\begin{bmatrix} p_{11} & 0 & 0 \\ 0 & p_{12} & 0 \\ 0 & 0 & p_{12} \end{bmatrix}$	[100]: Longitudinal
	c_{44}	$2\begin{bmatrix} 0 & p_{44} & 0 \\ p_{44} & 0 & 0 \\ 0 & 0 & 0 \end{bmatrix}$	[010]: Transverse
	c_{44}	$2\begin{bmatrix} 0 & 0 & p_{44} \\ 0 & 0 & 0 \\ p_{44} & 0 & 0 \end{bmatrix}$	[001]: Transverse
[110]	$\dfrac{c_{11}+c_{12}+2c_{44}}{2}$	$\begin{bmatrix} p_{11}+p_{12} & 2p_{44} & 0 \\ 2p_{44} & p_{11}+p_{12} & 0 \\ 0 & 0 & 2p_{12} \end{bmatrix}$	[110]: Longitudinal
	c_{44}	$\sqrt{2}\begin{bmatrix} 0 & 0 & p_{44} \\ 0 & 0 & p_{44} \\ p_{44} & p_{44} & 0 \end{bmatrix}$	[001]: Transverse
	$\dfrac{c_{11}-c_{12}}{2}$	$\begin{bmatrix} p_{11}-p_{12} & 0 & 0 \\ 0 & -(p_{11}-p_{12}) & 0 \\ 0 & 0 & 0 \end{bmatrix}$	[$\bar{1}$10]: Transverse
[111]	$\dfrac{c_{11}+2c_{12}+4c_{44}}{3}$	$\dfrac{2}{3}\begin{bmatrix} p_{11}+2p_{12} & 2p_{44} & 2p_{44} \\ 2p_{44} & p_{11}+2p_{12} & 2p_{44} \\ 2p_{44} & 2p_{44} & p_{11}+2p_{12} \end{bmatrix}$	[111]: Longitudinal
	$\dfrac{c_{11}-c_{12}+c_{44}}{3}$	$\dfrac{2}{\sqrt{6}}\begin{bmatrix} p_{11}-p_{12} & 0 & p_{44} \\ 0 & -(p_{11}-p_{12}) & -p_{44} \\ p_{44} & -p_{44} & 0 \end{bmatrix}$	[1$\bar{1}$0]: Transverse
	$\dfrac{c_{11}-c_{12}+c_{44}}{3}$	$\dfrac{2}{\sqrt{18}}\begin{bmatrix} p_{11}-p_{12} & 2p_{44} & -p_{44} \\ 2p_{44} & p_{11}-p_{12} & -p_{44} \\ -p_{44} & -p_{44} & -2(p_{11}-p_{12}) \end{bmatrix}$	[11$\bar{2}$]: Transverse

The present studies were carried out in two scattering geometries. In the "right-angle" scattering geometry θ is $\sim 90° \pm 5°$ and in the "back-scattering" geometry $\sim 165° \pm 10°$. For right-angle scattering, the sample was mounted on a spectrometer table which allowed angles to be measured to one minute of arc. After correcting for refraction at the crystal surfaces and for nonalignment of the sample along the Fabry-Perot axis,[20] our estimated error in scattering angle is $\sim 5'$. In the back-scattering geometry we study the Brillouin

shifts as a function of phonon propagation direction in the vicinity of a symmetry direction of the crystal. This was achieved by mounting the sample on a goniometer[21] which allowed us to measure scattering angles to within $6'$.

An effect that becomes important in a material like diamond, which has a high refractive index, is the presence of a reflected laser beam from the exit surface of the crystal. In the case of diamond this beam is approximately one-sixth as intense as the incident one. The reflected beam will also

TABLE II. Intensities (I) of Brillouin components for light incident along [110] and scattered along [$\bar{1}$10], the phonon propagation direction $\vec{q}$ being along [100]. H (horizontal) and V (vertical) denote the polarizations with respect to the horizontal scattering plane. Superscript and subscript refer to the scattered and incident polarizations, respectively.

$\vec{u}$	I_V^V	I_V^H	I_H^V	I_H^H
L: [100]	$\dfrac{4p_{12}^2}{c_{11}}$	0	0	$\dfrac{(p_{12}-p_{11})^2}{c_{11}}$
T: [010]	0	0	0	0
T: [001]	0	$\dfrac{2p_{44}^2}{c_{44}}$	$\dfrac{2p_{44}^2}{c_{44}}$	0

give rise to scattered radiation, and if retroreflection is assumed, the internal scattering angle will be complementary to that of the incident beam. For right-angle scattering the difference in scattering angle is usually small enough that the two peaks will not be resolved; however, an estimate can be made as to how much the peak will be shifted and a rough correction made. These corrections turn out to be very small, but they do improve the internal consistency of our results. All the experiments in this investigation were performed at ~ 295 °K.
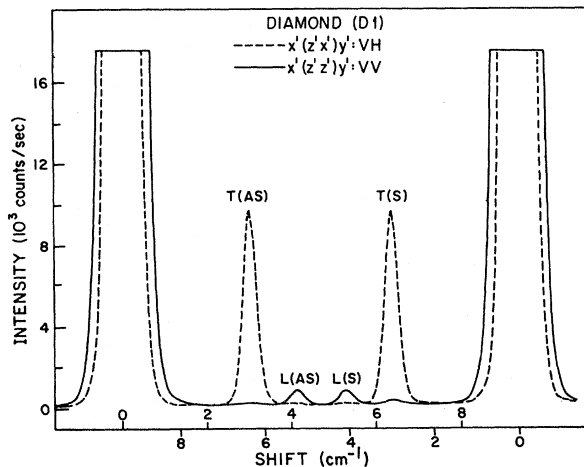
FIG. 1. Brillouin spectrum of diamond observed with a triple-passed scanning Fabry-Perot interferometer and excited with the multimode 4880-Å Ar$^+$ radiation incident along x' ∥ [110] and scattered along y' ∥ [$\bar{1}$10]; z' ∥ [001]. The scales below and above the base line refer to the shifts of the Stokes (S) and anti-Stokes (AS) components, respectively. In the labels VH and VV the first and second letters denote the polarization (V—vertical, H—horizontal) of the incident and scattered light, respectively, with respect to the horizontal, (001), scattering plane. T (transverse) and L (longitudinal) give the polarization characteristics of the phonon responsible for the scattering. The measurement was made at room temperature.
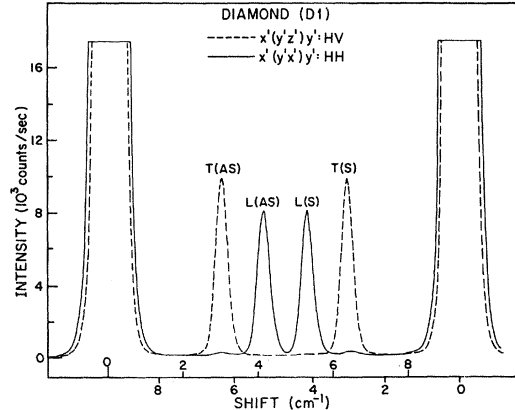
FIG. 2. Conditions under which this spectrum was taken are identical to those described in Fig. 1 except that the incident polarization is horizontal.

IV. EXPERIMENTAL RESULTS AND DISCUSSION

The Brillouin spectrum of diamond excited with 4880-Å radiation incident along [110] and scattered along [$\bar{1}$10] is shown in Figs. 1 and 2. For this scattering geometry, the phonon responsible for the scattering has its propagation direction along [100]; as can be seen from Table I, a pure longitudinal and a doubly degenerate pure transverse phonon can propagate along this direction. The Brillouin components were identified from the magnitude and sign of their frequency shifts and a knowledge of the elastic moduli; the labels T, L, H, V, S, and AS stand for transverse, longitudinal, horizontal, vertical, Stokes, and anti-Stokes, respectively. The observed polarization features can be compared with the predictions of Table II for this scattering geometry. The disappearance of the lines labeled T in the HH and VV polarizations and of those labeled L in the HV and VH polarizations strikingly confirms the assignments. As expected, the intensities of the transverse components are equal in the HV and VH polarizations. The relative intensity of the transverse to the longitudinal component, $I_T : I_L$, observed with incident light vertically polarized yields (p_{44}^2/c_{44}) $(c_{11}/2p_{12}^2)$. Similarly, $I_T : I_L$ for incident light horizontally polarized yields $(2p_{44}^2/c_{44})$ $[c_{11}/(p_{12}-p_{11})^2]$. The simultaneous observation of both the transverse and longitudinal components when no analyzer is used in the above measurements permits a reliable determination of the above intensity ratios, since the effects of changes in laser intensity and finesse can be minimized. From the experimental intensity ratios and the values of the elastic moduli determined in the present study, we have obtained $|p_{44}/p_{12}|$ and $|p_{44}/(p_{11}-p_{12})|$, and deduced $|p_{12}/(p_{11}-p_{12})|$. It is of interest to compare these ratios with those computed from the values of p_{ij}'s

TABLE III. Elasto-optic constants of diamond.[a]

p_{ij}	Ramachandran[b]	Ramachandran[c]	Denning et al.[d]	Grodzinski-Fisher[e]	Schneider[f]	Go et al.[g]
p_{11}	− 0.42	− 0.49	− 0.244	⋯	(− 0.249)	⋯
p_{12}	+ 0.27	+ 0.196	+ 0.042	⋯	(+ 0.043)	⋯
p_{44}	− 0.162	− 0.162	− 0.172	− 0.218	(− 0.172)	− 0.172
$p_{11}-p_{12}$	− 0.688	− 0.688	− 0.292	− 0.381	(− 0.292)	− 0.283
$p_{11}+2p_{12}$	+ 0.12	− 0.10	− 0.160	⋯	− 0.1640	− 0.16

[a]In this table we have computed, where necessary, the p_{ij}'s from the q_{ij}'s determined by the various workers using the c_{ij}'s of Ref. 8. With the exception of Schneider (Ref. 26), none of the investigators report dispersion of the elasto-optic constants.

[b]Reference 22. The absolute path differences used in this reference have been recalculated using the c_{ij}'s of Ref. 8 rather than those of Ref. 32.

[c]Reference 22. The absolute path difference was not corrected as in b. In most of the literature, e.g., Ref. 9, the p_{ij}'s are calculated without the correction mentioned above.

[d]Reference 23.

[e]The q_{ij}'s from which these are calculated are given in Ref. 23.

[f]Reference 26. The values in parentheses are obtained using $p_{11}-p_{12}$ and p_{44} from Ref. 23 together with $p_{11}+2p_{12}$ of Ref. 26 for $\lambda=5461$. This wavelength is close to that used by Denning et al. (Ref. 23).

[g]Reference 25.

given in the literature. Table III contains the p_{ij}'s determined by various workers[22-26] or calculated by us from their piezo-optic constants (q_{ij}). In Table IV we give ratios of suitable combinations of p_{ij}'s computed from the values given in Table III and compare them with the values obtained in the present investigation for 5145-Å excitation. As can be seen, the values of the ratios obtained in this study are in agreement with those of columns 3–6 in Table IV. We have also measured the absolute value of the constants p_{44} and $p_{11}-p_{12}$ by comparing the intensities of the Brillouin components in diamond with that of toluene.[27] We obtained $|p_{44}| = 0.18 \pm 0.04$ and $|p_{11}-p_{12}| = 0.31 \pm 0.06$, in very good agreement with the values of Denning et al.[23] We feel that the results in column 6, Table III, are the most reliable experimental values of elasto-optic constants of diamond because they combine the most accurate results of Denning et al.[23] for $p_{11}-p_{12}$ and p_{44} with that for $p_{11}+2p_{12}$ as given by Schneider.[26]

The relative intensities of Brillouin components

for phonon propagation directions other than the one discussed above can be used as further checks on the values of the elasto-optic constants. For this purpose we used right-angle scattering with the phonon propagation direction $\vec{q}$ confined to the $(1\bar{1}0)$ plane. It can be shown that for such a $\vec{q}$ there exists a pure transverse phonon polarized along $[1\bar{1}0]$ and a quasitransverse (QT) and a quasilongitudinal (QL) phonon polarized in the $(1\bar{1}0)$ plane. The polarization directions for the QT and QL phonons were computed by solving the Christoffel equations using the elastic moduli determined in this section. Once the propagation and polarization directions of the phonon are known the scattering tensor can be constructed in a straightforward manner. In Table V we present the intensity ratios of Brillouin components we have measured using the 5145-Å exciting radiation. It is clear that most of the experimental values and the ratios calculated using the p_{ij}'s of column 6, Table III, are in agreement. The discrepancies arise in two of the cases because of the difference between almost equal terms in the

TABLE IV. Ratios of elasto-optic constants of diamond.[a]

Ratios \ Ref.	b	c	d	e	f	g	Present study
$\left\|\dfrac{p_{44}}{p_{12}-p_{11}}\right\|$	0.235	0.236	0.589	0.572	0.589	0.608	0.572 ± 0.009
$\left\|\dfrac{p_{44}}{p_{12}}\right\|$	0.600	0.820	4.095	⋯	4.00	4.195	3.66 ± 0.09
$\left\|\dfrac{p_{12}}{p_{12}-p_{11}}\right\|$	0.392	0.286	0.144	⋯	0.147	0.145	0.156 ± 0.007

[a]Refs. b–g correspond to those given in Table III. The values quoted for the present study are for 5145-Å excitation.

TABLE V. Intensity ratios of Brillouin components for different directions of incident ($\vec{k}_i$) and scattered ($\vec{k}_s$) light. The calculated values were obtained using p_{ij}'s from Table III, column 6. H—horizontal; V—vertical; T—transverse; QL—quasilongitudinal.

Intensity ratio	Calc.	Expt.
(i) $\vec{k}_i \parallel [1\bar{1}2]$, $\vec{k}_s \parallel [\bar{1}1\bar{1}]$, $\vec{q} \parallel [11b]$, $b = 4 + 3\sqrt{2}$		
$\dfrac{(I_V^H)_T}{(I_H^V)_T} = \dfrac{1}{2} \dfrac{(p_{12} - p_{11} + 2bp_{44})^2}{(p_{11} - p_{12} + bp_{44})^2}$	1.11	0.95 ± 0.04
$\dfrac{(I_H^V)_T}{(I_H^V)_{QL}} = 2(\sqrt{2} - 1)^2 \dfrac{(p_{11} - p_{12} + bp_{44})^2}{[3.76(p_{11} - p_{12}) + 0.9492p_{44}]^2} \dfrac{X_{QL}}{X_T}$	1.19	1.17 ± 0.04
$\dfrac{(I_V^H)_T}{(I_V^H)_{QL}} = \dfrac{(\sqrt{2} - 1)^2}{18} \dfrac{[-(p_{11} - p_{12}) + 2bp_{44}]^2}{(0.0388p_{11} + 1.9576p_{12} - 0.0776p_{44})^2} \dfrac{X_{QL}}{X_T}$	15.2	8.8 ± 0.5
$X_{QL} = 10.922 \times 10^{12}$ dyn/cm^2; $X_T = 5.751 \times 10^{12}$ dyn/cm^2		
(ii) $\vec{k}_i \parallel [111]$; $\vec{k}_s \parallel [\bar{1}\bar{1}2]$; $\vec{q} \parallel [11b]$; $b = 4 - 3\sqrt{2}$		
$\dfrac{(I_V^H)_T}{(I_H^V)_T} = 2 \dfrac{[(p_{11} - p_{12}) + bp_{44}]^2}{[-(p_{11} - p_{12}) + 2bp_{44}]^2}$	0.89	0.87 ± 0.03
$\dfrac{(I_H^V)_T}{(I_H^V)_{QL}} = \dfrac{(\sqrt{2} + 1)^2 [-(p_{11} - p_{12}) + 2bp_{44}]^2}{[-1.8028(p_{11} - p_{12}) - 4.8764p_{44}]^2} \dfrac{X_{QL}}{X_T}$	1.09	1.03 ± 0.02
$\dfrac{(I_V^H)_T}{(I_V^H)_{QL}} = \dfrac{(\sqrt{2} + 1)^2}{9} \dfrac{[(p_{11} - p_{12}) + bp_{44}]^2}{(0.9669p_{11} + 1.0324p_{12} - 1.9338p_{44})^2} \dfrac{X_{QL}}{X_T}$	5.4	7.8 ± 0.2
$X_{QL} = 11.854 \times 10^{12}$ dyn/cm^2; $X_T = 4.804 \times 10^{12}$ dyn/cm^2		
(iii) $\vec{k}_i \parallel [001]$, $\vec{k}_s \parallel [110]$, $\vec{q} \parallel [11\sqrt{2}]$		
$\dfrac{(I_V^H)_T}{(I_H^V)_T} = \dfrac{4p_{44}^2}{(p_{11} - p_{12})^2}$	1.39	1.26 ± 0.03
$\dfrac{(I_H^V)_T}{(I_H^V)_{QL}} = \dfrac{(p_{11} - p_{12})^2}{(-1.9986p_{44})^2} \dfrac{X_{QL}}{2X_T}$	0.83	1.00 ± 0.01
$\dfrac{(I_V^H)_T}{(I_V^H)_{QL}} = \dfrac{2p_{44}^2}{(0.5175p_{11} + 1.4811p_{12} - 1.0350p_{44})^2} \dfrac{X_{QL}}{X_T}$	10.6	11.0 ± 0.6
$X_{QL} = 12.04 \times 10^{12}$ dyn/cm^2; $X_T = 5.256 \times 10^{12}$ dyn/cm^2		
(iv) $\vec{k}_i \parallel [100]$, $\vec{k}_s \parallel [010]$, $\vec{q} \parallel [1\bar{1}0]$		
$\dfrac{(I_H^V)_T}{(I_H^V)_L} = \dfrac{c_{11} + c_{12} + 2c_{44}}{4c_{44}}$	1.02	1.06 ± 0.05
$\dfrac{(I_V^H)_T}{(I_V^V)_L} = \dfrac{p_{44}^2}{p_{12}^2} \dfrac{c_{11} + c_{12} + 2c_{44}}{4c_{44}}$	16.3	13.6 ± 1.5

denominators of the calculated ratios.

The wavelength dependence of the p_{ij}'s has been studied by various authors. Ramachandran[22] found no dispersion in the region from 5893 to 4358 Å and Poindexter[28] found no change in q_{44} in the region from 7700 to 4400 Å. Schneider,[26] however, found $p_{11} + 2p_{12}$ to vary from -0.1586 at 5893 Å to -0.2033 at 3663 Å. We measured the ratios $|p_{11}/(p_{11} - p_{12})|$ and $|p_{44}/p_{12}|$ at various wavelengths and our results are summarized in Table VI. From the results in this table it is not clear whether the ratio $|p_{44}/(p_{11} - p_{12})|$ shows any appreciable dispersion, but $|p_{44}/p_{12}|$ has a definite wavelength dependence. If we assume that p_{44} and p_{11} have

little dispersion, our results would imply that the absolute value of p_{12} decreases with decreasing wavelength. Schneider's results are consistent with the above interpretation.

Figure 3 shows the experimental results obtained for different incident wavelengths for the same geometry as that of Figs. 1 and 2, the incident light being horizontally polarized. The Brillouin shifts increase with decreasing wavelength, in agreement with Eq. (1), with v_s assumed to be a constant; i.e., the elastic constants do not show any dispersion within our experimental accuracy. The differences in intensity of a Brillouin component for different excitation lines are, in the main, due

TABLE VI. Ratios of elasto-optic constants as a function of wavelength.

Ratio \ Wavelength (Å)	6328	5145	4880	4579
$\left\lvert\dfrac{p_{44}}{p_{11}-p_{12}}\right\rvert$	0.58 ± 0.03	0.572 ± 0.009	0.572 ± 0.007	0.551 ± 0.009
$\left\lvert\dfrac{p_{44}}{p_{12}}\right\rvert$	$\cdots$	3.66 ± 0.09	3.85 ± 0.09	4.8 ± 0.2

to the differences of the incident power, the λ^{-4} dependence of the scattered intensity, and the sensitivity of the photomultiplier, and, to a lesser extent, due to filter and mirror characteristics. The small differences in the intensity of the Stokes and anti-Stokes components seen in the figure are of known instrumental origin and not physically significant.

The measurements of frequency shifts were carried out as described in Sec. III using small free-spectral ranges (~ 0.5 cm^{-1}). With these free-spectral ranges the differences in interference order (Δn) between the unshifted radiation and the Brillouin components is typically in the neighborhood of 7; as can be seen from Eq. (3), this large Δn significantly improves the accuracy of the measured $\Delta\tilde{\nu}$. The error affecting a given measurement arises from errors in (i) the measured fractional order, (ii) the free-spectral range, (iii) the measured scattering angle, and (iv) the uncertainty in $\vec{q}/|\vec{q}|$ and hence in the appropriate combination of c_{ij}'s.

We assume errors in (i), (ii), and (iii) to be random, giving rise to the experimentally determined spread in the measured values of X. Error in (iv), on the other hand, will not be random, because it depends on the accuracy with which the crystal faces are polished normal to the specified directions. The corresponding correction due to this effect can be estimated by computing the variations in X as a function of angle within the range by which $\vec{q}/|\vec{q}|$ may differ from the desired direction. This is accomplished by solving the secular determinant using approximate values for c_{ij}'s. It should be noted that, if for the direction under study, X is either a maximum or a minimum, the resulting correction will be considerably smaller. It is for this reason that we mostly studied symmetry directions. For right-angle scattering the error due to this last effect is $\sim\frac{1}{3}$ that due to the other three. For back scattering, on the other hand, the error in (iv) turns out to be the dominant one. It should be noted that if X is determined as a function of the angle (γ) between the phonon propagation direction and the normal to the crystal face, a maximum or a minimum should be obtained for it along a symmetry direction. For example,
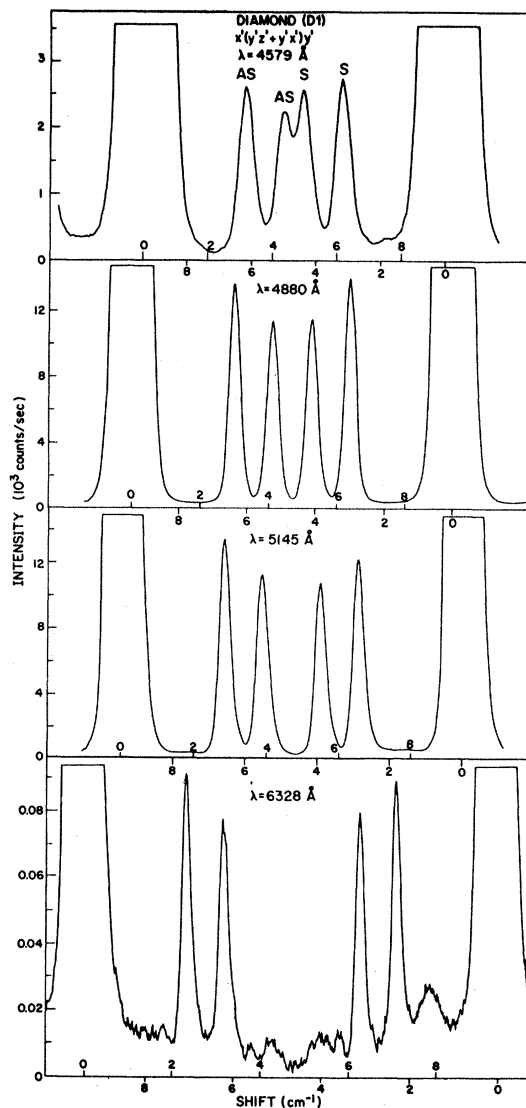
FIG. 3. Brillouin scattering of diamond as a function of the wavelength of the exciting radiation. The scattering geometry and the free spectral range are the same as those in Figs. 1 and 2, with the light horizontally polarized. The scales below and above the base lines refer to the shifts of the Stokes (S) and anti-Stokes (AS) components, respectively. The power of the multimode 4579-, 4880-, 5145-, and 6328-Å exciting radiation is ~ 100, 950, 1200, and 75 mW, respectively.

TABLE VII. Elastic moduli of diamond from Brillouin scattering (units: 10^{12} dyn/cm^2).

| Scattering geometry | | | Phonon | X | | |
$\vec{k}_i$	$\vec{k}_s$	$\vec{q}$	Polarization	Theory	Experiment	Least–squares fit
[110]	[$\bar{1}$10]	[100]	L	c_{11}	10.78 ± 0.02	10.764 ± 0.002
[110]	[$\bar{1}$10]	[100]	T	c_{44}	5.774 ± 0.015	5.774 ± 0.014
[001]	[110]	[11$\sqrt{2}$]	T	$\frac{1}{4}(c_{11} - c_{12} + 2c_{44})$	5.27 ± 0.05	5.265 ± 0.013
[111]	[$\bar{1}\bar{1}\bar{1}$]	[111]	L	$\frac{1}{3}(c_{11} + 2c_{12} + 4c_{44})$	12.121 ± 0.002	12.121 ± 0.035
[001]	[00$\bar{1}$]	[001]	L	c_{11}	10.764 ± 0.002	10.764 ± 0.002
[110]	[$\bar{1}\bar{1}$0]	[110]	L	$\frac{1}{2}(c_{11} + c_{12} + 2c_{44})$	11.80 ± 0.01	11.782 ± 0.027

we obtained X as a function of γ in the (001) plane in the vicinity of the [110] direction of $\vec{q}$ and observed a maximum; fixing the [$\bar{1}$10] direction of the crystal, γ is now varied in the ($\bar{1}$10) plane. The results are shown in Fig. 4, where the observed minimum is taken to be along the [110] direction. The fact that the minimum occurs at $\gamma \sim 1.5°$ shows that the specified crystallographic direction [110] departs to that extent from the normal to the surface of the crystal. In Table VII we give the experimental determinations of X's for the different scattering geometries we have studied. These values were obtained with 5145- and/or 4880-Å exciting radiation. The values quoted are averages of several measurements. Attention should be drawn to the increased accuracy obtained in back scattering over right-angle scattering, and for a symmetry direction over a nonsymmetry direction. In the calculation of X's using Eq. (1) we have taken $\rho = 3.512$ g/cm^3, following McSkimin and Bond[29]; the refractive indices at 5145 and 4880 Å were obtained using the dispersion formula of Peter.[30] It is clear from Table VII that the value of c_{11} obtained in the back-scattering geometry along [001] is very precise and also does not appear in combination with other c_{ij}'s. Selecting this as our best value for c_{11}, we determined c_{44} and c_{12} by performing a least-squares fit on the X's in Table VII using the procedure of DuMond and Cohen.[31] These values are given in Table VIII; the combinations of c_{ij}'s appearing in Table VII have been recalculated using these values and are presented under the column labeled "least-squares fit." The agreement between the experimental values and those given by the least-squares fit demonstrates the internal consistency of our results.

In Table VIII we compare the c_{ij}'s for diamond determined by various workers. As can be seen, our results are in excellent agreement with those of McSkimin and Andreatch,[8] who used the ultrasonic-pulse technique; it is very gratifying to see that the accuracy attainable with the current techniques of Brillouin scattering is comparable to that of the ultrasonic-pulse method. The improvements

in Brillouin-scattering techniques due to the introduction of lasers and scanning interferometers no doubt account for the differences between our results and those of Ref. 7. McSkimin and Bond[29] have discussed the relative merits of the ultrasonic-wedge method[32] and the ultrasonic-pulse method, and have concluded that the latter should yield more accurate results. The elastic modulus c_{11} determined by Prince and Wooster[33] using diffuse scattering of x rays agrees with our value within the errors quoted; however, their values for c_{12} and c_{44} do not agree with ours, even allowing for the error brackets and the temperature dependence of c_{ij}'s as given by McSkimin and Andreatch.[8] The Debye temperature Θ_D, calculated for 0 °K using our elastic constants and the procedure given by de Launay,[34] is (2246 ± 5) °K. This is in excellent agreement with the low-temperature Θ_D, (2246 ± 15) and (2219 ± 20) °K, as determined by Burk and Friedberg[35] and Desnoyers and Morrison,[36] respectively. This agreement had already been noted by these workers, using the elastic mod-
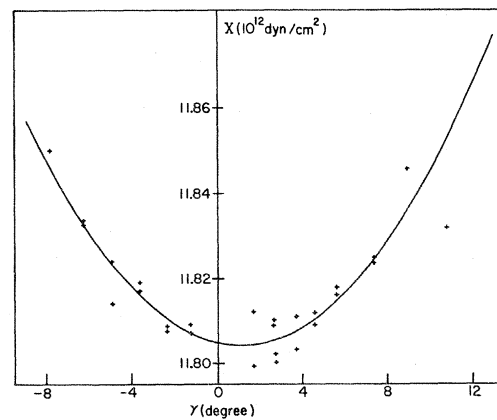
FIG. 4. Effective elastic modulus X as a function of the angle (γ) between the phonon propagation direction and the normal to the crystal face, in the vicinity of $\vec{q} \parallel$ [110] and γ in the ($\bar{1}$10) plane. The solid curve represents a least-squares fit of a second-order polynomial to the experimental data.

TABLE VIII. Elastic moduli of diamond (units: 10^{12} dyn/cm^2).

Method	c_{11}	c_{12}	c_{44}	Ref.
Brillouin scattering (~23 °C)	10.764 ± 0.002	1.252 ± 0.023	5.774 ± 0.014	Present study; Ref. 10
Brillouin scattering	9.49	1.51	5.21	7
X-ray diffuse scattering (300 °C)	11.0 ± 1.1	3.3 ± 0.3	4.4 ± 0.4	33
Ultrasonic-wedge method	9.5	3.9	4.3	32
Ultrasonic-pulse technique (25 °C)	10.79 ± 0.05	1.24 ± 0.05	5.78 ± 0.02	8

uli of McSkimin and Bond,[29] which in turn are in excellent agreement with ours. The bulk modulus $K = \frac{1}{3}(c_{11} + 2c_{12})$ calculated from our elastic moduli is $(4.42 \pm 0.02) \times 10^{12}$ dyn/cm^2; the experimental values for K are 6.3 and 5.6 in units of 10^{12} dyn/cm^2, as determined by Adams[37] and Williamson,[38] respectively. Also, the calculated Young modulus (Y)[39] in the (111) plane is 11.64×10^{12} dyn/cm^2 compared to 5.5×10^{12} dyn/cm^2 as measured by Pisharoty.[40] We feel that both K and Y should be remeasured before any physical significance can be given to the above discrepancies.

In Fig. 5 we present the Brillouin and first-order Raman spectrum of diamond measured under identical conditions with a double monochromator.[16] The scattering geometry $z'(y'x'+y'z')y'$ was used to obtain these results, where x', y', and z' are along $[\bar{1}10]$, $[110]$, and $[001]$, respectively, x' being vertical. At room temperature, the Stokes and anti-Stokes Brillouin components are expected to be equally intense; the small difference in intensity noticed in the figure is thought to be of instrumental origin, since the monochromator was used at the limit of its capabilities. For this scattering geometry the Brillouin component with the smaller shift is essentially pure transverse, the quasitransverse being ~250 times weaker; the component with the larger frequency shift is clearly the quasilongitudinal (QL). Also, the Raman line and the QL Brillouin component appear only in the $I_{\mathrm{H}}^{\mathrm{H}}$ spectrum. The Raman-scattering efficiency per unit crystal length per unit solid angle in the $I_{\mathrm{H}}^{\mathrm{H}}$ spectrum is given by[41]

$$S_{\mathrm{Raman}} = \frac{2\hbar\omega_s^4 N^2 a^2}{\rho c^4 \omega_j}(n_0 + 1) \ , \tag{4}$$

where ω_j is the frequency of the zone-center optical phonon[3] $[= 2\pi c (1332)\,\mathrm{rad/sec}]$; $\omega_s = \omega_L - \omega_j$; n_0 is the Bose population factor; N is the number of primitive cells per unit volume $(= 8.87 \times 10^{22}/\mathrm{cm}^3)$; a is the single independent component characterizing the Raman tensor per unit cell. The scattering efficiency of the QL Brillouin component per unit crystal length per unit solid angle is[1]

$$S_{\mathrm{Brillouin\ QL}} = n^8 \frac{kT\omega_s^4}{128\pi^2 c^4} \frac{(-1.9986 p_{44})^2}{X_{\mathrm{QL}}} \ , \tag{5}$$

where $\omega_s = \omega_L - \omega_{\mathrm{QL}}$ and $X_{\mathrm{QL}} = 12.04 \times 10^{12}$ dyn/cm^2.

The ratio of the integrated intensities of the Raman line and the QL Brillouin component in Fig. 5 is measured to be 7.1 ± 0.9. From Eqs. (4) and (5) and using $p_{44} = -0.172$ we obtain $|a| = 4.4 \pm 0.3$ Å^2. This is in excellent agreement with the measurements of Anastassakis and Burstein,[41] who obtained values in the range 3.4–4.4 Å^2 from the electric-field-induced infrared absorption, and with the measurements of McQuillan et al.,[42] who obtained 4.6 Å^2 from absolute intensity measurements. Maradudin and Burstein[43] have deduced a theoretical expression relating a to the p_{ij}'s which was found,[41] using the p_{ij}'s of Ramachandran,[22] to be in agreement with the previously mentioned results. However, using the more recent values of p_{ij}'s as given in Table III, column 6, their expression yields $a = +0.53$ instead of -3.8 Å^2; this discrepancy needs to be resolved by further study.

ACKNOWLEDGMENTS

FIG. 5. Brillouin and first-order Raman spectrum of diamond with light incident along z' ∥ $[001]$, and scattered along y' ∥ $[110]$, with x' ∥ $[\bar{1}10]$ being vertical. The spectrum was recorded with 5145-Å Ar$^+$ exciting radiation and at room temperature. The data presented in this figure have been corrected for the instrument function.

---

*Work supported by the National Science Foundation under Grant No. GH32001A1 and MRL Program Nos. GH 33574A1 and GH 33574A3.

[1] R. Loudon, Adv. Physics **13**, 423 (1964).

[2] H. Z. Cummins and P. E. Schoen, in *Laser Handbook*, edited by F. T. Arecchi and E. O. Schulz-Dubois (North-Holland, Amsterdam, 1972), p. 1029.

[3] S. A. Solin and A. K. Ramdas, Phys. Rev. B **1**, 1687 (1970).

[4] J. L. Warren, J. L. Yarnell, G. Dolling, and R. A. Cowley, Phys. Rev. **158**, 805 (1967).

[5] R. S. Krishnan, Proc. Ind. Acad. Sci. A **26**, 399 (1947).

[6] V. Chandrasekharan, Proc. Ind. Acad. Sci. A **32**, 379 (1950).

[7] R. S. Krishnan, V. Chandrasekharan, and E. S. Rajagopal, Nature Lond. **182**, 518 (1958).

[8] H. J. McSkimin and P. Andreatch, J. Appl. Phys. **43**, 2944 (1972).

[9] See Table I in R. S. Leigh and B. Szigeti, J. Phys. C **3**, 782 (1970).

[10] Preliminary results were presented in M. H. Grimsditch and A. K. Ramdas, Physics Lett. A **48**, 37 (1974). The corrections arising from any nonalignment of the Fabry-Perot axis with respect to the collection optics were not taken into account in this paper. This has been incorporated in the present paper.

[11] V. Chandrasekharan, Proc. Ind. Acad. Sci. A **33**, 183 (1951); J. Phys. Radium **26**, 655 (1965).

[12] V. Chandrasekharan, Proc. Natl. Inst. Sci. **19**, 547 (1953).

[13] These specimens are obtained from the Diamond Research Laboratory, Industrial Distributors (1946) Ltd., Johannesburg, South Africa.

[14] Model FP-100 Fabry-Perot Interferometer, Tropel Inc., 52 West Ave., Fairport, N. Y., 14450.

[15] J. R. Sandercock, in *Light Scattering in Solids*, edited by M. Balkanski (Flammarion, Paris, 1971), p. 9.

[16] Model 25-100 double monochromator, Jarrell-Ash Division, 590 Lincoln Street, Waltham, Mass. 02154.

[17] S. A. Solin, Ph.D. thesis (Purdue University, 1970) (unpublished).

[18] G. E. Devlin, J. L. Davis, L. Chase, and S. Geschwind, Appl. Phys. Lett. **19**, 138 (1971).

[19] The following spectral lines were used for the determination of the free spectral range. (i) Fine structure of the 5460.7-Å line of Hg. We used the wavelengths given by Jobin Yvon, 163 Avenue Gambetta, 75980 Paris, Cedex 20, France, in their brochure on the type THR 1500 monochromator. (ii) Ne lines at 6334.4279, 6328.173 Å and at 5852.4878, 5881.8950, 5944.8342 Å; these values were obtained from *MIT Wavelength Tables* (MIT Press, Cambridge, Mass., 1969). (iii) Hg lines at 5769.5982, 5790.6630 Å; these values were obtained from *American Institute of Physics Handbook* (McGraw-Hill, New York, 1972). The above group of lines were isolated using interference filters at 5450, 6328, 5896, and 5780 Å, respectively. The Hg lines were obtained from a GE type G4T4-1 lamp and the Ne lines from a Westinghouse hollow-cathode K-lamp (in neon atmosphere) type WL-22863A.

[20] The details of this procedure will be given in M. H. Grimsditch, Ph.D. thesis (Purdue University) (unpublished).

[21] Model 250 goniometer manufactured by South Bay Technology, Inc., 4900 Santa Anita Avenue, El Monte, Calif. 91731.

[22] G. N. Ramachandran, Proc. Ind. Acad. Sci. **32A**, 171 (1950).

[23] R. M. Denning, A. A. Giardini, E. Poindexter, and C. B. Slawson, Am. Min. **42**, 556 (1957).

[24] P. Grodzinski and Fisher, quoted by Denning *et al.*, in Ref. 23.

[25] S. Go, H. Bilz, and M. Cardona (private communication).

[26] W. C. Schneider, Ph.D. thesis (Pennsylvania State University, 1970) (unpublished). This author has reviewed the measurements of E. D. D. Schmidt, J. L. Kirk, and K. Vedam, Am. Min. **53**, 1404 (1968).

[27] L. Benckert and G. Bäckström, Phys. Rev. B **8**, 5888 (1973). For the convenience of matching intensities and shifts, the Brillouin components of diamond were first compared with the Brillouin line of glycerin and this in turn with the line of toluene.

[28] E. Poindexter, Am. Min. **40**, 1032 (1955).

[29] H. J. McSkimin and W. L. Bond, Phys. Rev. **105**, 116 (1957).

[30] F. Peter, Z. Phys. **15**, 358 (1923).

[31] J. W. M. DuMond and E. R. Cohen, Rev. Mod. Phys. **25**, 691 (1953); see also E. R. Cohen, Rev. Mod. Phys. **25**, 709 (1953).

[32] S. Bhagavantam and J. Bhimasenachar, Proc. R. Soc. Lond. A **187**, 381 (1946).

[33] E. Prince and W. A. Wooster, Acta. Cryst. **6**, 450 (1953).

[34] J. de Launay, J. Chem. Phys. **24**, 1071 (1956).

[35] D. L. Burk and S. A. Friedberg, Phys. Rev. **111**, 1275 (1958).

[36] J. E. Desnoyers and J. A. Morrison, Phil. Mag. **3**, 42 (1958).

[37] L. H. Adams, J. Wash. Acad. Sci. **11**, 45 (1921).

[38] E. D. Williamson, J. Franklin Inst. **193**, 491 (1922).

[39] J. F. Nye, *Physical Properties of Crystals* (Oxford U. P., London, 1964), p. 145.

[40] P. R. Pisharoty, Proc. Ind. Acad. Sci. A **12**, 208 (1940).

[41] E. Anastassakis and E. Burstein, Phys. Rev. B **2**, 1952 (1970). A factor of $\frac{2}{3}$ has been included because the incident light is horizontally polarized. The scattered radiation in our experiment not being along a cubic axis does not modify Eq. (4).

[42] A. K. McQuillan, W. R. L. Clements, and B. P. Stoicheff, Phys. Rev. A **1**, 628 (1970). It should be noted that the expression used in this reference for the Raman scattering efficiency is for unpolarized incident light, the incident and scattered light being along orthogonal cubic axes. For other scattering geometries this expression must be suitably modified. See L. Couture and J. P. Mathieu, Ann. Phys. **3**, 521 (1948).

[43] A. A. Maradudin and E. Burstein, Phys. Rev. **164**, 1081 (1967).